Eur J Nucl Med Mol Imaging (2016) 43:526–536
DOI 10.1007/s00259-015-3222-3

ORIGINAL ARTICLE

Does posterior cingulate hypometabolism result from disconnection or local pathology across preclinical and clinical stages of Alzheimer's disease?

Stefan Teipel[1,2] · Michel J. Grothe[2] · for the Alzheimer´s Disease Neuroimaging Initiative

Received: 10 July 2015 / Accepted: 7 October 2015 / Published online: 10 November 2015

Abstract
Purpose Posterior cingulate cortex (PCC) hypometabolism as measured by FDG PET is an indicator of Alzheimer's disease (AD) in prodromal stages, such as in mild cognitive impairment (MCI), and has been found to be closely associated with hippocampus atrophy in AD dementia. We studied the effects of local and remote atrophy and of local amyloid load on the PCC metabolic signal in patients with different preclinical and clinical stages of AD.
Methods We determined the volume of the hippocampus and PCC grey matter based on volumetric MRI scans, PCC amyloid load based on AV45 PET, and PCC metabolism based on FDG PET in 667 subjects participating in the Alzheimer's Disease Neuroimaging Initiative spanning the range from cognitively normal ageing through prodromal AD to AD dementia.
Results In cognitively normal individuals and those with early MCI, PCC hypometabolism was exclusively associated with hippocampus atrophy, whereas in subjects with late MCI it was associated with both local and remote effects of atrophy as well as local amyloid load. In subjects with AD dementia, PCC hypometabolism was exclusively related to local atrophy.
Conclusion Our findings suggest that the effects of remote pathology on PCC hypometabolism decrease and the effects of local pathology increase from preclinical to clinical stages of AD, consistent with a progressive disconnection of the PCC from downstream cortical and subcortical brain regions.

Keywords Early diagnosis · Prodromal Alzheimer's disease · Hippocampus atrophy · Multimodal imaging · Amyloid pathology · Disconnection

Introduction

Posterior cingulate cortex (PCC) hypometabolism has repeatedly been identified as an early marker of Alzheimer's disease (AD) on FDG PET examinations [1, 2]. Several studies have indicated that the metabolic reduction in the PCC in AD dementia is related to disrupted input from connected regions that undergo early atrophy in the course of AD, such as the hippocampus [3, 4]. This notion is supported by the association between PCC hypometabolism in AD dementia and atrophy of the cingulate bundle that connects the PCC and the hippocampus [5–7]. A potential pathophysiological mechanism for this association has been found in previous PET studies demonstrating remote effects of a regional lesion on neuronal metabolism in distant brain structures, such as in crossed cerebellar diaschisis after supratentorial stroke [8, 9], or reduced PCC metabolism after experimentally induced medial temporal lobe lesions in monkeys [10]. However, PCC hypometabolism in AD dementia may also be reflective of pathological processes within the PCC itself, such as local

Data used in the preparation of this article were obtained from the Alzheimer's Disease Neuroimaging Initiative (ADNI) database (http://adni.loni.usc.edu/). As such, the investigators within the ADNI contributed to the design and implementation of ADNI and/or provided data but did not participate in the analysis of the data or the writing of this report. A complete list of ADNI investigators can be found at: http://adni.loni.usc.edu/wp-content/uploads/how_to_apply/ADNI_Acknowledgement_List.pdf

✉ Stefan Teipel
stefan.teipel@med.uni-rostock.de

[1] Department of Psychosomatic Medicine, University of Rostock, Rostock, Germany

[2] DZNE, German Center for Neurodegenerative Diseases, Gehlsheimer Str. 20, 18147 Rostock, Germany

grey matter (GM) atrophy or amyloid toxicity [11, 12]. So far, the association between PCC hypometabolism and local and remote effects of atrophy has mainly been studied in the dementia stages of AD [3–5], but not yet in preclinical or prodromal stages of the disease. Moreover, the relative contribution of local amyloid pathology to PCC hypometabolism has not yet been studied in this context.

Based on the previous findings, we assumed that the PCC FDG PET signal represents a convolution of local and remote pathological effects whose contributions vary across different preclinical and clinical stages of AD. Here, we used combined structural MRI and multitracer PET data from the ADNI to study the association between PCC hypometabolism and local amyloid load and local and remote atrophy in a large sample of individuals spanning the range from cognitively normal (CN) ageing through prodromal AD to AD dementia.

Materials and methods

Data source

Data used in the preparation of this article were obtained from the ADNI database (http://adni.loni.usc.edu/). The ADNI was launched in 2003 by the National Institute on Aging, the National Institute of Biomedical Imaging and Bioengineering, the Food and Drug Administration, private pharmaceutical companies and nonprofit organizations, with the primary goal of testing whether neuroimaging and neuropsychological and other biological measurements can be used as reliable in vivo markers of AD pathogenesis. A fuller description of ADNI and up-to-date information is available at www.adni-info.org.

Study participants

AV45 PET, FDG PET and structural MRI scans were retrieved from the ADNI-GO and ADNI-2 extensions of the ADNI project and included imaging data from 179 CN elderly subjects (CN group), 269 subjects with mild cognitive impairment (MCI) in early stages (early stage MCI, EMCI group), 134 subjects in later more advanced stages of MCI (LMCI group) and 85 subjects in dementia stages of AD (AD group). The subjects' demographics are shown in Table 1.

Detailed inclusion criteria for the diagnostic categories can be found on the ADNI website (http://adni.loni.usc.edu/methods/). Briefly, CN subjects have a MMSE score in the range 24 – 30 and a clinical dementia rating (CDR) of 0, and are nondepressed, non-MCI and nondemented. EMCI subjects have a MMSE score in the range 24 – 30, a subjective memory concern reported by the subject, informant or clinician, objective memory loss measured in terms of education-adjusted scores on delayed recall (one paragraph from Wechsler Memory Scale Logical Memory II; education-adjusted scores 9 – 11 if ≥16 years of age, 5 – 9 if 8 – 15 years of age, and 3 – 6 if 0 – 7 years of age), a CDR of 0.5, absence of significant levels of impairment in other cognitive domains, essentially preserved activities of daily living, and absence of dementia. The diagnosis of LMCI differs from that of EMCI only in a higher degree of objective memory impairment (education adjusted scores ≤8 if ≥16 years of age, ≤4 if 8 – 15 years of age, ≤2 if 0 – 7 years of age). Subjects with AD dementia have an initial MMSE score in the range 20 – 26, a CDR of 0.5 or 1.0, and fulfil NINCDS-ADRDA criteria for clinically probable AD [13].

For additional analyses, CN and EMCI subjects were dichotomized into amyloid-low and amyloid-high groups, using a cortex-to-whole cerebellum standardized uptake value ratio (SUVR) threshold of ≥1.17 that has been suggested to be indicative of pathological levels of amyloid associated with AD based on combined antemortem AV45 PET and postmortem neuropathological examination [14]. Cortex-to-whole cerebellum AV45 SUVRs have been calculated by one of the ADNI PET core laboratories (Jagust Lab, UC Berkeley [15]) and are available for download on the ADNI server.

Imaging data acquisition

ADNI-GO/ADNI-2 MRI data were acquired on multiple 3-T MRI scanners using scanner-specific T1-weighted sagittal 3-D MPRAGE sequences. In order to increase signal uniformity among the multicentre scanner platforms, original MPRAGE acquisitions in ADNI undergo standardized image preprocessing correction steps. AV45 and FDG PET data were acquired on multiple instruments of various resolutions and following different platform-specific acquisition protocols. Similar to the MRI data, PET data in ADNI undergo standardized image preprocessing correction steps aimed at increasing data uniformity among the multicentre acquisitions. More detailed information on the different imaging protocols employed at the ADNI sites and standardized image preprocessing steps for MRI and PET acquisitions can be found on the ADNI website (http://adni.loni.usc.edu/methods/).

Imaging data processing

Imaging data were processed using statistical parametric mapping (SPM8; Wellcome Trust Center for Neuroimaging) and the VBM8 toolbox (http://dbm.neuro.uni-jena.de/vbm/) implemented in MATLAB R2013b (MathWorks, Natick, MA).

MRI data processing

First, MRI scans were automatically segmented into GM, white matter (WM) and cerebrospinal fluid (CSF) partitions

Table 1 Subjects' demographics

Group	No. of subjects	Age (years)		Gender (F/M)[a]	Education (years)		MMSE score	
		Mean±SD	Significant differences ($p<0.05$)		Mean±SD	Significant differences ($p<0.05$)	Mean±SD	Significant differences ($p<0.05$)
AD	85	75.6±8.3	–	36/49	15.7±2.8	vs. CN group	22.9±2.0	vs. CN group
LMCI	134	72.4±8.1	vs. AD group	62/72	16.5±2.7	vs. AD group	27.5±1.9	vs. CN group and LMCI group
EMCI	269	71.4±7.4	vs. CN group and AD group	121/148	15.9±2.7	vs. CN group and LMCI group	28.4±1.6	vs. CN group, AD group and LMCI group
CN	179	73.8±6.5	–	91/88	16.6±2.5	–	29.1±1.2	–

MMSE Mini-Mental State Examination

[a] No significant overall effect, chi-squared=2.2, $p=0.53$

of isotropic voxel size 1.5 mm using the tissue prior free segmentation routine of the VBM8 toolbox. The resulting GM and WM partitions of each subject in native space were then high-dimensionally registered to an ageing/AD-specific reference template from a previous study [16] using DARTEL [17]. Structural brain characteristics change considerably with advancing age and in AD and spatial registration accuracy worsens with deviation from the template characteristics, rendering the MNI standard space template inappropriate for high-dimensional deformation-based morphometry studies of aged and demented populations. Therefore, the reference template in this study was derived using DARTEL by aligning 50 healthy elderly subjects and 50 subjects with very mild, mild and moderate AD retrieved from an open access MRI database (www.oasis-brains.org), and thus reflects unbiased ageing/AD-specific structural characteristics. Individual flow fields resulting from the DARTEL registration to the reference template were used to warp the GM segments and voxel values were adjusted for volumetric changes introduced by the high-dimensional normalization, such that the total amount of GM volume present before warping was preserved.

PET data processing

Each subject's AV45 and FDG PET scans were rigidly coregistered to a skull-stripped version of the corresponding structural MRI scan and corrected for partial volume effects (PVE). PVE correction was performed using the algorithm proposed by Müller-Gärtner et al. [18] and was implemented using MATLAB scripts written in-house based on the image processing routines of SPM8. Briefly, the algorithm consists of correcting the GM PET signal for both signal spill-out effects and spill-in effects from the surrounding tissue. The PET signal in WM and CSF compartments was measured as the average signal within the individual WM and CSF partitions, thresholded at 99 % tissue probability. Only regions with a GM probability of at least 50 % were retained in the PVE-corrected AV45 and FDG PET scans. GM-specific PVE-corrected PET scans in subject space were spatially normalized to the reference template (without adjustment of voxel values) using the DARTEL flow fields derived from the registration of the corresponding MRI scans. For voxel-based analyses the warped PET scans were smoothed with a Gaussian smoothing kernel of 8 mm full-width at half-maximum.

Extraction of imaging features from hippocampus and posterior cingulate regions of interest

Figure 1 shows the hippocampus and PCC regions of interest (ROIs) projected onto the reference template. The hippocampal ROI mask was obtained by manual delineation of the hippocampus in the reference template using the interactive software package Display (McConnell Brain Imaging Centre at the Montreal Neurological Institute) and a previously described protocol for segmentation of the medial temporal lobe [19].

The ROI mask for the PCC was derived from the Harvard–Oxford structural brain atlas [20]. The PCC label was high-dimensionally warped into the reference space of this study using DARTEL registration parameters of the MNI152 template (the template space of the Harvard–Oxford structural atlas), and the warped label was multiplied with a binary GM mask of the reference template, thresholded at 50 % GM probability. Individual GM volumes of the ROIs were extracted automatically from the warped GM segments by summing the adjusted GM voxel values within the respective ROI masks in the reference space. For further analysis, the extracted regional GM volumes were scaled by the total intracranial volume, calculated as the sum of the total volume of the GM, WM and CSF partitions.

Individual AV45 and FDG PET uptake values of the PCC were extracted from the warped PET maps by averaging the voxel values within the intersection between the PCC mask and the warped PET maps in the reference space. Mean regional FDG and AV45 PET uptake values were converted to SUVRs by scaling to the mean uptake value within a mask of

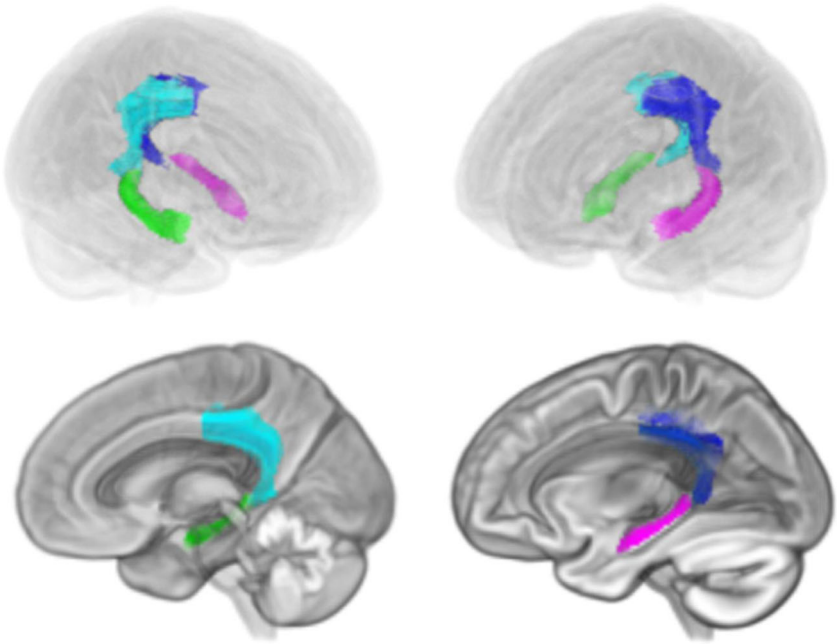

Fig. 1 Hippocampal and PCC regions of interest. The anatomical locations of the left (*violet*) and right (*green*) hippocampus and the left (*blue*) and right (*cyan*) PCC regions of interest are shown in transparent views (*top*) and midsagittal and left sagittal slices (*bottom*) of the rendered study template. Images were created using MRIcroGL software (http://www.mccauslandcenter.sc.edu/mricrogl/)

cerebellar GM derived from the Hammers Maximum Probability atlas [21].

Statistics

Between-group effects for age and education were evaluated using Student's *t*-test, for MMSE score using the Mann–Whitney *U* test, and for sex using the chi-squared statistic. Metabolic, amyloid and volume measurements were compared between groups using ANCOVA models, controlling for age and sex, with pair-wise follow-up tests using the post-hoc Scheffé test. The main effects of hippocampus and PCC volumes and amyloid signal on PCC metabolism and interaction effects with group were assessed in ANCOVA models controlling for age and sex. Within each diagnostic group, associations between hippocampus, PCC amyloid load and PCC GM volume with PCC metabolism were determined using partial correlations controlling for age and gender. Separate models were calculated for each diagnostic group and hemisphere. The squared partial correlation coefficients were used as effect size estimates for the associations. When more than one modality was significantly associated with PCC metabolism, partial correlation and the Sobel test were used to test for a mediation effect.

Results

Between-group effects

Between-group differences in demographic variables are shown in Table 1. In the ANCOVA models, all volumetric and PET variables showed a significant overall effect across the four groups (CN, EMCI, LMCI, AD dementia) at $F(3, 663)>24$, $p<0.001$. The post hoc pair-wise analysis showed significant differences in hippocampus volumes among all the groups with AD<LMCI<EMCI<CN for both hemispheres ($p<0.023$, post hoc Scheffé test). For the PCC, GM volume effects were AD<LMCI<EMCI=CN for both hemispheres ($p<0.017$ for the significant differences). Group effects for PCC metabolism were AD<LMCI<EMCI=CN for both hemispheres ($p<0.001$ for the significant differences). The PCC amyloid signal was AD>LMCI>EMCI=CN for both hemispheres ($p<0.005$ for the significant differences).

Association with PCC metabolism

For both hemispheres, the overall model showed significant main effects of hippocampus and PCC volumes on the PCC metabolic signal ($F(1, 648)>5.6$, $p<0.02$), but no significant main effect of the PCC AV45 PET signal ($F(1, 648)<0.5$, $p>0.48$). The interaction between group and PCC volume on PCC metabolic signal was significant ($F(3, 648)>4.8$, $p<0.002$), but there were no significant interaction effects of group by hippocampus volume or PCC AV45 PET signal ($F(3, 648)<2.1$, $p>0.10$).

We followed this overall effect within each group. Squared partial correlation coefficients as effect size estimates and levels of significance are shown in Table 2, and scatter plots of group-specific effects are shown in Fig. 2. In the CN and EMCI subjects, for both hemispheres only hippocampus volume was significantly associated with PCC metabolism. In the LMCI subjects, hippocampus volume and PCC volume as well as AV45 PET signal were significantly associated with

Table 2 Percent squared partial correlation coefficients for the associations between predictors (hippocampus and PCC volumes, and AV45 PET signal in the PCC) and the PVE-corrected PCC FDG PET signal in the corresponding hemisphere, controlling for age and sex

Group	Hippocampus volume		PCC volume		PVE-corrected AV45 PET PCC signal	
	Left	Right	Left	Right	Left	Right
Controls	4.5**	4.0*	0.0	0.0	0.0	0.0
EMCI	2.1*	1.8*	0.0	0.0	0.0	0.0
LMCI	11.8***	10.1***	11.7***	7.6***	3.2*	4.5*
AD	0.0	0.0	18.3***	28.7***	0.0	2.3

*$p<0.05$, **$p<0.005$, ***$p<0.001$

PCC metabolism. In AD patients, for both hemispheres only PCC volume was associated with PCC metabolism.

Only in the LMCI subjects did more than one modality contribute to the metabolic signal of the PCC. Therefore, we restricted the mediation analysis to the LMCI group. After controlling for the volumetric measures, the effect of AV45 PCC signal on FDG PCC signal was lost, whereas the effect of both volumes (hippocampus and PCC) was retained after controlling for the other volume and the AV45 signal. The Sobel test was significant ($t=-2.65$, $p<0.01$) for PCC GM volume mediating the local AV45 effect (Fig. 3). Hippocampus volume was not a significant mediator of the local AV45 effect ($t=-1.83$, $p=0.066$).

For further analysis the CN, EMCI and LMCI groups were stratified according to global amyloid load. There were significant positive correlations between the AV45 PET signal and the FDG PET signal in amyloid-low CN subjects in the right hemisphere (partial $r=0.18$, $p<0.05$) and in amyloid-low EMCI subjects in both hemispheres (partial $r=0.15$ and 0.24 for left and right, respectively; $p<0.05$). There were no significant effects in amyloid-high or amyloid-low LMCI subjects, or in amyloid-high CN and EMCI subjects (Fig. 4). Only in LMCI subjects was global amyloid load significantly negatively associated with local PCC metabolic signal (partial $r=-0.20$, $p<0.03$, for both hemispheres), and not in the CN, EMCI and AD dementia subjects.

Discussion

In our analysis, the contribution of local and remote pathological effects on the PCC metabolic signal varied among CN,

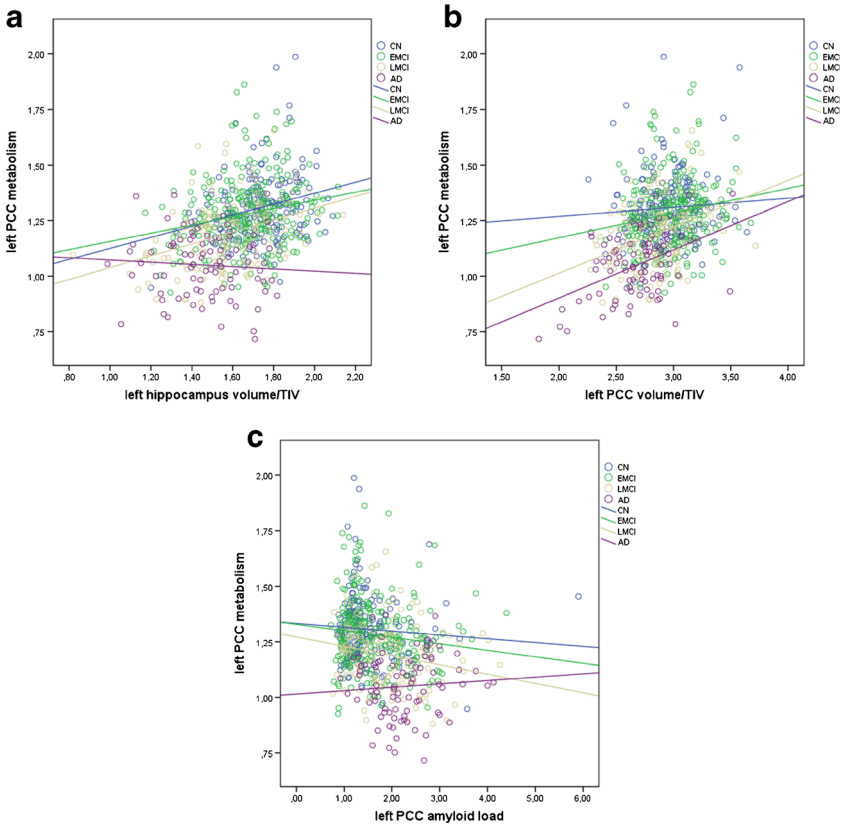

Fig. 2 Correlations between volumes, amyloid load and PCC metabolism Scatter plots and least square regression lines for the regression of PCC FDG PET metabolic signal on **a** total intracranial volume-normalized left hippocampus volume, **b** normalized left PCC volume, and **c** PCC amyloid load in the CN, EMCI, LMCI and AD dementia groups

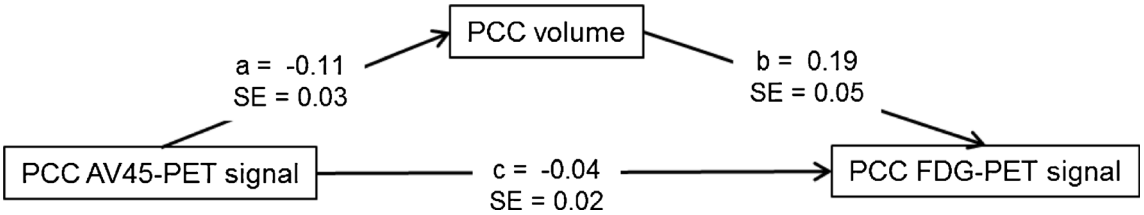

Fig. 3 PCC GM volume mediates the effect of the PCC AV45 PET signal on PCC FDG PET signal in LMCI subjects. Direct effect of PCC amyloid on PCC metabolism and indirect effect via PCC grey matter volume: *a* regression coefficient for the effect of PCC AV45 PET signal on PCC volume; *b* regression coefficient for the effect of PCC volume on PCC FDG PET signal after controlling for the effect of PCC AV45 PET signal on PCC FDG PET signal; *c* regression coefficient for the effect of PCC AV45 PET signal on PCC FDG PET signal (*SE* standard error)

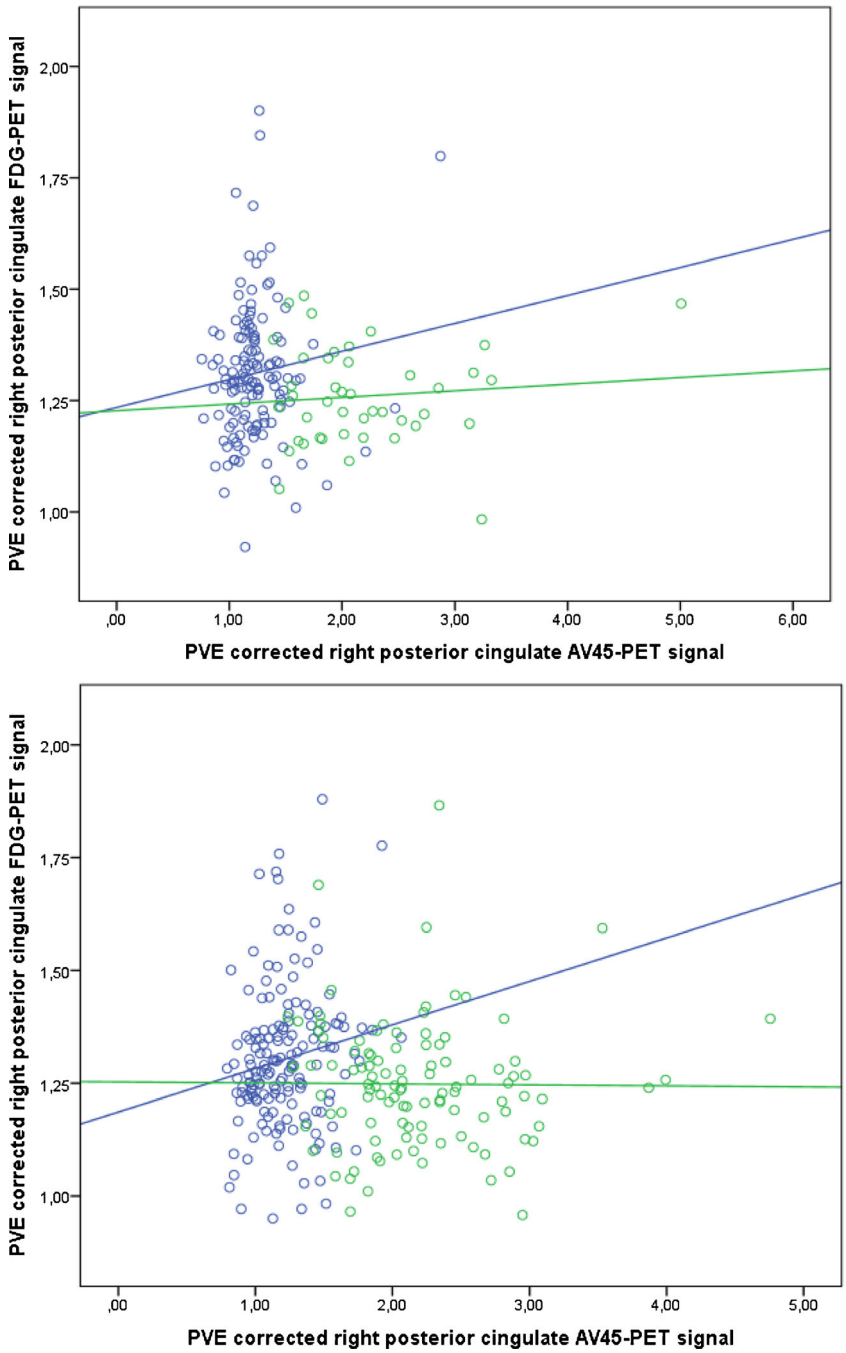

Fig. 4 PCC amyloid and metabolic signal according to global amyloid load. Scatter plots and least square regression lines for the regression of PCC FDG PET metabolic signal on PCC AV45 PET signal in (*top*) CN subjects and (*bottom*) EMCI subjects (*blue* global amyloid-negative subjects, *green* global amyloid-positive subjects)

EMCI, LMCI and AD subjects. In CN and EMCI subjects, the PCC metabolic signal was associated with hippocampus volume, but independent of local amyloid load and atrophy. In LMCI subjects, with clinically more advanced disease, remote atrophy and local amyloid load and atrophy contributed to the PCC metabolic signal, whereas in AD subjects, only local atrophy was a significant predictor of the PCC FDG PET signal. We discuss below the associations between PCC hypometabolism and local and hippocampus atrophy, the inverse associations between PCC metabolic signal and amyloid signal, and the positive associations between amyloid load and metabolism in the PCC.

Our findings extend previous reports on the association between metabolic decline in PCC and hippocampus atrophy in AD [3, 4]. Our findings suggest that this effect is stage-dependent: it is most pronounced in clinically healthy ageing and predementia stages of AD, but is lost in clinically manifest AD dementia. In contrast, local atrophy was the only significant determinant of the PCC metabolic signal in AD dementia patients, consistent with a previous analysis of voxel-wise correlations between hypometabolism and atrophy in 20 AD dementia patients [22]. Local atrophy contributed to the metabolic signal in individuals with advanced MCI stages, but not in those with early MCI or in clinically healthy controls. In cognitively healthy controls, the association between hippocampus volume and the PCC FDG PET signal suggests that PCC metabolic activity is coupled to the activity of connected areas such as the hippocampus. This is in line with a large body of evidence from resting-state functional MRI studies demonstrating a synchronous coupling of intrinsic activity fluctuations in the medial temporal lobe and the PCC [23]. With advancing stages of AD pathology, the PCC and hippocampus become increasingly disconnected as shown by disruption of fibres of the cingulum bundle on diffusion tensor imaging [24, 25], as well as an uncoupling of intrinsic activity fluctuations between the two sites in resting-state functional MRI data [26, 27]. In these advanced stages, the influence from medial temporal areas on PCC metabolism may be widely lost, and variations in PCC metabolism may be mainly driven by local levels of atrophy. This interpretation also agrees with the previous observation that the integrity of the cingulum bundle alters the functional association between the hippocampus and PCC in AD dementia cases [5].

The local AV45 PET signal was inversely associated with PCC metabolism in subjects with LMCI in this study. This contrasts with the findings of a study in a small sample of 21 subjects with MCI that showed no significant association between amyloid PET and FDG PET signal in the PCC [28]; we could not find any other studies in subjects with MCI addressing the local association between amyloid and FDG PET signal in the PCC. In contrast to LMCI subjects, we found no significant associations between local amyloid load and PCC metabolic signal in AD dementia subjects. This agrees with the findings of a study in 20 AD dementia patients that showed only a small cluster of significant positive voxel-wise correlations in the PCC between amyloid and metabolic signal at an uncorrected level of significance [22], and the findings of another study in 39 AD dementia patients that showed no significant association between local amyloid and metabolism in a ROI-based analysis [29]. Our finding contrasts with significant negative correlations between parietal cortex amyloid and FDG PET signal found in two previous studies with small samples of 16 and 10 AD dementia patients, respectively [30, 31]. Two other studies showed an inverse association between local amyloid and PCC metabolic signal [32, 33]. However, these effects were assessed in combined groups of healthy controls, and MCI and AD dementia patients, and thus may have been driven mainly by clinical group effects.

A previous study points to a potential mechanism that may account for the differences between LMCI and AD dementia patients in the associations between PCC amyloid and metabolic signal. AD dementia patients showed a moderate increase in goodness-of-fit of the hypometabolic pattern with the spatial pattern of amyloid deposition when the FDG PET scan after 2 years follow-up was compared with baseline amyloid scans [34]. These data were interpreted as showing that the metabolic decline in AD dementia follows the regional distribution of amyloid accumulation with some temporal delay. Amyloid load was shown to increase linearly in preclinical and prodromal stages of AD, but to plateau in the dementia stage of AD [35]. Such an effect would explain why we did not find a direct association between local amyloid load and local FDG PET signal in a cross-sectional analysis of the AD dementia patients: in AD dementia, the variation in local amyloid would no longer be the driver of the variation in local glucose uptake at a given time-point. In contrast, in the MCI stage of AD an association between local amyloid and FDG PET signal would prevail due to the preserved dynamics of amyloid accumulation.

In CN and EMCI subjects we found no significant associations between local amyloid load and PCC metabolism. The absence of an effect in the CN control subjects agrees with the findings of two previous studies that showed no association in amyloid-positive controls [36] or in healthy controls without a parental history of AD dementia [37]. However, in contrast to our present findings, a recent study in a large cohort of elderly CN subjects did show significant negative associations between local amyloid levels and metabolic signal in several AD-typical regions, including the PCC [11].

In a secondary analysis, we stratified our CN, EMCI and LMCI subjects according to global amyloid load. This analysis was inspired by two previous studies that had shown positive associations between amyloid load and FDG metabolism. In one study such an association was seen in 14 amyloid-positive MCI patients, but not in 14 amyloid-

positive CN controls [36], and in the other study in 81 CN controls [38] including amyloid-positive and amyloid-negative patients. Interestingly, we found such an effect only in the absence of an overall increased amyloid load in the CN and EMCI subjects. This finding points to two different mechanisms that potentially underlie the positive association between local amyloid and metabolism in the PCC. The first hypothesis is that a local increase in amyloid in the PCC, an area that builds up amyloid early in the course of the disease [39], results in an increase in local metabolism. Such an effect has also been demonstrated in a transgenic animal model of cerebral amyloid accumulation [40]. This interpretation agrees with the notion that Aβ peptides, including Aβ42 and Aβ40, the main constituents of amyloid plaques, play a physiological role in synaptic plasticity [41]. Thus, amyloid may act in a nonlinear fashion on local metabolism, a surrogate marker of synaptic activity [42], where at lower levels of accumulation, it stimulates local metabolism, but at higher levels has a detrimental effect on local metabolism [43]. An alternative explanation is based on the regulation of Aβ release through synaptic activity. Higher synaptic activity has been found to lead to higher levels of soluble Aβ species in ex vivo brain slices [44]. Such an effect would be relevant as long as the metabolic activity in the PCC is not yet suppressed by advanced disease mechanisms. Indeed, with more advanced disease, in our LMCI subjects there were no longer positive local associations between metabolic signal and amyloid load.

Synaptic activity-induced amyloid release has already been suggested as a possible mechanism to account for the early involvement of metabolically active cortical regions in amyloid accumulation, as indicated by multimodal imaging studies [45]. The AV45 tracer florbetapir is believed to bind to fibrillary Aβ, bound in amyloid plaques [46], rather than to Aβ monomers and oligomers that are considered to interact with synaptic activity [47]. Therefore, a direct link between in vivo PET findings and potentially underlying neurobiological changes at the synaptic level is not possible, and the underlying mechanisms explaining our findings cannot be resolved from the imaging data alone. In addition, a recent study [48] in 54 CN subjects showed that people with more pronounced amyloid load showed no difference in levels of atrophy and hypometabolism compared with people with lower amyloid load, even at a very liberal level of significance ($p<0.05$, uncorrected). In contrast, people with more pronounced markers of neurodegeneration (combined from atrophy and metabolism) showed less amyloid accumulation in a voxel-based analysis. These data point to a potential selection bias in a group of elderly CN subjects in whom both increased amyloid load and impaired metabolism and volume are unlikely to be present in the absence of cognitive decline.

The study had some limitations. First, although we interpreted our findings in a stage-specific manner, we acknowledge that these are cross-sectional data that potentially could have been contaminated by secular effects. Longitudinal data on the interaction between atrophy, FDG PET, and amyloid PET changes in predementia and preclinical stages of AD are based on small sample sizes and the regional interplay between the different modalities over time have not yet been examined [49]. Second, based on the notion that EMCI subjects perform between healthy elderly and LMCI subjects in episodic memory, it is reasonable to assume that EMCI is a transition stage between healthy ageing and more advanced MCI. However, evidence for this assumption is still lacking. In all between-group comparisons except hippocampus volume, the EMCI subjects were similar to the healthy CN controls, underscoring the heterogeneity of this clinical concept. The lack of difference in PCC metabolism dissociates EMCI from the classical MCI concept in which PCC hypometabolism has been shown as a robust finding [50]. Third, effect sizes for the significant effects of hippocampus volume on PCC metabolism were small, particularly in CN and EMCI subjects. This observation suggests that in these cases PCC metabolism may be mainly driven by intrinsic physiological factors rather than by local or remote pathological events.

Finally, the use of PVE correction of PET data may have influenced our results. Given that PVEs may introduce spurious correlations between local atrophy and decreased hypometabolism, correction of the PET signal for PVEs is an important methodological requirement in studies aiming to assess the independence of the effect of local atrophy on hypometabolism (see, for example, Chetelat et al. [5]). However, PVE correction methods also depend on a range of model assumptions that may not always hold true or may only be roughly approximated in the imaging data [51, 52], and thus we cannot finally exclude the possibility that this procedure may have resulted in a possible undercorrection or even overcorrection of PVEs in our data. However, the employed PVE correction algorithm has been shown to efficiently increase the correspondence of the FDG PET signal with the true GM signal in simulated data, and to reduce spurious correlations between atrophy and hypometabolism in aged and demented subjects [18, 53–55]. Although PVE correction is still not commonly used for amyloid PET data, recent methodological studies have indicated that it increases the validity of the measured PET signal, particularly when using methods that control for spill-in effects of high nonspecific binding signal from WM areas, and its use is generally recommended for quantitative amyloid PET imaging [56, 57].

In summary, we found differential associations between local and remote pathological events and the FDG PET metabolic signal in the PCC in healthy ageing subjects, through subjects with predementia stages of AD to subjects with AD dementia. Hippocampus atrophy was the most relevant driver of PCC hypometabolism in the controls and EMCI subjects, probably reflecting a diaschisis-like phenomenon. In LMCI subjects, PCC hypometabolism was associated with remote

effects as well as with local atrophy and amyloid pathology, whereas in AD dementia subjects only local atrophy was significantly associated with local PCC hypometabolism. In LMCI subjects, local atrophy was a significant mediator of the local amyloid effect. In contrast, in EMCI subjects and controls, with normal levels of global amyloid, local amyloid was positively associated with local FDG PET signal in the PCC, possibly reflecting an interaction between synaptic activity and amyloid release at physiological levels of amyloid expression. The PCC metabolic signal represents a complex convolution of different physiological and pathological mechanisms across the stages of AD. Thus, it integrates over the influences of different remote and local pathologies in the MCI stage of AD; this may explain its high accuracy in the detection of this stage of disease in diagnostic PET studies. Future research integrating measures of structural and functional connectivity based on diffusion-weighted and functional MRI imaging will seek to corroborate the notion that the loss of connectivity between the PCC and downstream areas, such as the hippocampus, may drive the switch from predominantly remote to predominantly local effects on the PCC signal with disease progression.

Acknowledgments Data collection and sharing for this project was funded by the Alzheimer's Disease Neuroimaging Initiative (ADNI; National Institutes of Health grant U01 AG024904) and DOD ADNI (Department of Defense award number W81XWH-12-2-0012). The ADNI was launched in 2003 by the National Institute on Aging (NIA), the National Institute of Biomedical Imaging and Bioengineering (NIBIB), the Food and Drug Administration (FDA), private pharmaceutical companies and nonprofit organizations, as a $60 million, 5-year public–private partnership. ADNI is funded by the NIA, the NIBIB, and generous contributions from the following: Alzheimer's Association; Alzheimer's Drug Discovery Foundation; Araclon Biotech; BioClinica, Inc.; Biogen Idec Inc.; Bristol-Myers Squibb Company; Eisai Inc.; Elan Pharmaceuticals, Inc.; Eli Lilly and Company; EuroImmun; F. Hoffmann-La Roche Ltd and its affiliated company Genentech, Inc.; Fujirebio; GE Healthcare; IXICO Ltd.; Janssen Alzheimer Immunotherapy Research & Development, LLC.; Johnson & Johnson Pharmaceutical Research & Development LLC.; Medpace, Inc.; Merck & Co., Inc.; Meso Scale Diagnostics, LLC.; NeuroRx Research; Neurotrack Technologies; Novartis Pharmaceuticals Corporation; Pfizer Inc.; Piramal Imaging; Servier; Synarc Inc.; and Takeda Pharmaceutical Company. The Canadian Institutes of Health Research provides funds to support ADNI clinical sites in Canada. Private sector contributions are facilitated by the Foundation for the National Institutes of Health (www.fnih.org). The grantee organization is the Northern California Institute for Research and Education, and the study is coordinated by the Alzheimer's Disease Cooperative Study at the University of California, San Diego. ADNI data are disseminated by the Laboratory for Neuroimaging at the University of Southern California.

Compliance with ethical standards

Conflicts of Interest None.

Ethical approval All procedures performed in the ADNI studies involving human participants were in accordance with the ethical standards of the institutional research committees and with the principles of the 1964 Declaration of Helsinki and its later amendments.

Informed consent Written informed consent was obtained from all participants and/or authorized representatives and the study partners before any protocol-specific procedures were carried out in the ADNI study.

References

1. Minoshima S, Frey KA, Koeppe RA, Foster NL, Kuhl DE. A diagnostic approach in Alzheimer's disease using three-dimensional stereotactic surface projections of fluorine-18-FDG PET. J Nucl Med. 1995;36:1238–48.
2. Pagani M, De Carli F, Morbelli S, Oberg J, Chincarini A, Frisoni GB, et al. Volume of interest-based [18F]fluorodeoxyglucose PET discriminates MCI converting to Alzheimer's disease from healthy controls. A European Alzheimer's Disease Consortium (EADC) study. Neuroimage Clin. 2015;7:34–42. doi:10.1016/j.nicl.2014.11.007.
3. Yakushev I, Schreckenberger M, Muller MJ, Schermuly I, Cumming P, Stoeter P, et al. Functional implications of hippocampal degeneration in early Alzheimer's disease: a combined DTI and PET study. Eur J Nucl Med Mol Imaging. 2011;38:2219–27. doi:10.1007/s00259-011-1882-1.
4. Villain N, Desgranges B, Viader F, de la Sayette V, Mezenge F, Landeau B, et al. Relationships between hippocampal atrophy, white matter disruption, and gray matter hypometabolism in Alzheimer's disease. J Neurosci. 2008;28:6174–81. doi:10.1523/JNEUROSCI.1392-08.2008.
5. Chetelat G, Villain N, Desgranges B, Eustache F, Baron JC. Posterior cingulate hypometabolism in early Alzheimer's disease: what is the contribution of local atrophy versus disconnection? Brain. 2009;132:e133. doi:10.1093/brain/awp253. Author reply e134.
6. Villain N, Fouquet M, Baron JC, Mezenge F, Landeau B, de La Sayette V, et al. Sequential relationships between grey matter and white matter atrophy and brain metabolic abnormalities in early Alzheimer's disease. Brain. 2010;133:3301–14. doi:10.1093/brain/awq203.
7. Bozoki AC, Korolev IO, Davis NC, Hoisington LA, Berger KL. Disruption of limbic white matter pathways in mild cognitive impairment and Alzheimer's disease: a DTI/FDG-PET study. Hum Brain Mapp. 2012;33:1792–802. doi:10.1002/hbm.21320.
8. Nagasawa H, Kogure K, Fujiwara T, Itoh M, Ido T. Metabolic disturbances in exo-focal brain areas after cortical stroke studied by positron emission tomography. J Neurol Sci. 1994;123:147–53.
9. Akiyama H, Harrop R, McGeer PL, Peppard R, McGeer EG. Crossed cerebellar and uncrossed basal ganglia and thalamic diaschisis in Alzheimer's disease. Neurology. 1989;39:541–8.
10. Meguro K, Blaizot X, Kondoh Y, Le Mestric C, Baron JC, Chavoix C. Neocortical and hippocampal glucose hypometabolism following neurotoxic lesions of the entorhinal and perirhinal cortices in the non-human primate as shown by PET. Implications for Alzheimer's disease. Brain. 1999;122(Pt 8):1519–31.
11. Lowe VJ, Weigand SD, Senjem ML, Vemuri P, Jordan L, Kantarci K, et al. Association of hypometabolism and amyloid levels in aging, normal subjects. Neurology. 2014;82:1959–67. doi:10.1212/WNL.0000000000000467.
12. Ibanez V, Pietrini P, Alexander GE, Furey ML, Teichberg D, Rajapakse JC, et al. Regional glucose metabolic abnormalities are not the result of atrophy in Alzheimer's disease. Neurology. 1998;50:1585–93.
13. McKhann G, Drachman D, Folstein M, Katzman R, Price D, Stadlan EM. Clinical diagnosis of Alzheimer's disease: report of

the NINCDS-ADRDA Work Group under the auspices of the Department of Health and Human Services Task Force on Alzheimer's disease. Neurology. 1984;34:939–44.
14. Fleisher AS, Chen K, Liu X, Roontiva A, Thiyyagura P, Ayutyanont N, et al. Using positron emission tomography and florbetapir F18 to image cortical amyloid in patients with mild cognitive impairment or dementia due to Alzheimer disease. Arch Neurol. 2011;68:1404–11. doi:10.1001/archneurol.2011.150.
15. Landau SM, Breault C, Joshi AD, Pontecorvo M, Mathis CA, Jagust WJ, et al. Amyloid-beta imaging with Pittsburgh compound B and florbetapir: comparing radiotracers and quantification methods. J Nucl Med. 2013;54:70–7. doi:10.2967/jnumed.112.109009.
16. Grothe M, Heinsen H, Teipel SJ. Atrophy of the cholinergic basal forebrain over the adult age range and in early stages of Alzheimer's disease. Biol Psychiatry. 2012;71:805–13. doi:10.1016/j.biopsych.2011.06.019.
17. Ashburner J. A fast diffeomorphic image registration algorithm. Neuroimage. 2007;38:95–113.
18. Müller-Gärtner HW, Links JM, Prince JL, Bryan RN, McVeigh E, Leal JP, et al. Measurement of radiotracer concentration in brain gray matter using positron emission tomography: MRI-based correction for partial volume effects. J Cereb Blood Flow Metab. 1992;12:571–83.
19. Pruessner JC, Li LM, Serles W, Pruessner M, Collins DL, Kabani N, et al. Volumetry of hippocampus and amygdala with high-resolution MRI and three-dimensional analysis software: minimizing the discrepancies between laboratories. Cereb Cortex. 2000;10:433–42.
20. Desikan RS, Segonne F, Fischl B, Quinn BT, Dickerson BC, Blacker D, et al. An automated labeling system for subdividing the human cerebral cortex on MRI scans into gyral based regions of interest. Neuroimage. 2006;31:968–80. doi:10.1016/j.neuroimage.2006.01.021.
21. Hammers A, Allom R, Koepp MJ, Free SL, Myers R, Lemieux L, et al. Three-dimensional maximum probability atlas of the human brain, with particular reference to the temporal lobe. Hum Brain Mapp. 2003;19:224–47. doi:10.1002/hbm.10123.
22. La Joie R, Perrotin A, Barre L, Hommet C, Mezenge F, Ibazizene M, et al. Region-specific hierarchy between atrophy, hypometabolism, and beta-amyloid (Abeta) load in Alzheimer's disease dementia. J Neurosci. 2012;32:16265–73. doi:10.1523/JNEUROSCI.2170-12.2012.
23. Vincent JL, Snyder AZ, Fox MD, Shannon BJ, Andrews JR, Raichle ME, et al. Coherent spontaneous activity identifies a hippocampal-parietal memory network. J Neurophysiol. 2006;96:3517–31. doi:10.1152/jn.00048.2006.
24. Stahl R, Dietrich O, Teipel SJ, Hampel H, Reiser MF, Schoenberg SO. White matter damage in Alzheimer disease and mild cognitive impairment: assessment with diffusion-tensor MR imaging and parallel imaging techniques. Radiology. 2007;243:483–92. doi:10.1148/radiol.2432051714.
25. Fischer FU, Scheurich A, Wegrzyn M, Schermuly I, Bokde AL, Kloppel S, et al. Automated tractography of the cingulate bundle in Alzheimer's disease: a multicenter DTI study. J Magn Reson Imaging. 2012;36:84–91. doi:10.1002/jmri.23621.
26. Pasquini L, Scherr M, Tahmasian M, Meng C, Myers NE, Ortner M, et al. Link between hippocampus' raised local and eased global intrinsic connectivity in AD. Alzheimers Dement. 2015;11:475–84. doi:10.1016/j.jalz.2014.02.007.
27. Tahmasian M, Pasquini L, Scherr M, Meng C, Forster S, Mulej Bratec S, et al. The lower hippocampus global connectivity, the higher its local metabolism in Alzheimer disease. Neurology. 2015;84:1956–63. doi:10.1212/WNL.0000000000001575.
28. Forsberg A, Engler H, Almkvist O, Blomquist G, Hagman G, Wall A, et al. PET imaging of amyloid deposition in patients with mild cognitive impairment. Neurobiol Aging. 2008;29:1456–65. doi:10.1016/j.neurobiolaging.2007.03.029.
29. Furst AJ, Rabinovici GD, Rostomian AH, Steed T, Alkalay A, Racine C, et al. Cognition, glucose metabolism and amyloid burden in Alzheimer's disease. Neurobiol Aging. 2012;33:215–25. doi:10.1016/j.neurobiolaging.2010.03.011.
30. Engler H, Forsberg A, Almkvist O, Blomquist G, Larsson E, Savitcheva I, et al. Two-year follow-up of amyloid deposition in patients with Alzheimer's disease. Brain. 2006;129:2856–66. doi:10.1093/brain/awl178.
31. Edison P, Archer HA, Hinz R, Hammers A, Pavese N, Tai YF, et al. Amyloid, hypometabolism, and cognition in Alzheimer disease: an [11C]PIB and [18F]FDG PET study. Neurology. 2007;68:501–8. doi:10.1212/01.wnl.0000244749.20056.d4.
32. Drzezga A, Becker JA, Van Dijk KR, Sreenivasan A, Talukdar T, Sullivan C, et al. Neuronal dysfunction and disconnection of cortical hubs in non-demented subjects with elevated amyloid burden. Brain. 2011;134:1635–46. doi:10.1093/brain/awr066.
33. Li Y, Rinne JO, Mosconi L, Pirraglia E, Rusinek H, DeSanti S, et al. Regional analysis of FDG and PIB-PET images in normal aging, mild cognitive impairment, and Alzheimer's disease. Eur J Nucl Med Mol Imaging. 2008;35:2169–81.
34. Forster S, Grimmer T, Miederer I, Henriksen G, Yousefi BH, Graner P, et al. Regional expansion of hypometabolism in Alzheimer's disease follows amyloid deposition with temporal delay. Biol Psychiatry. 2012;71:792–7. doi:10.1016/j.biopsych.2011.04.023.
35. Villemagne VL, Burnham S, Bourgeat P, Brown B, Ellis KA, Salvado O, et al. Amyloid beta deposition, neurodegeneration, and cognitive decline in sporadic Alzheimer's disease: a prospective cohort study. Lancet Neurol. 2013;12:357–67. doi:10.1016/S1474-4422(13)70044-9.
36. Cohen AD, Price JC, Weissfeld LA, James J, Rosario BL, Bi W, et al. Basal cerebral metabolism may modulate the cognitive effects of Abeta in mild cognitive impairment: an example of brain reserve. J Neurosci. 2009;29:14770–8. doi:10.1523/JNEUROSCI.3669-09.2009.
37. Mosconi L, Rinne JO, Tsui WH, Murray J, Li Y, Glodzik L, et al. Amyloid and metabolic positron emission tomography imaging of cognitively normal adults with Alzheimer's parents. Neurobiol Aging. 2013;34:22–34. doi:10.1016/j.neurobiolaging.2012.03.002.
38. Ossenkoppele R, Madison C, Oh H, Wirth M, van Berckel BN, Jagust WJ. Is verbal episodic memory in elderly with amyloid deposits preserved through altered neuronal function? Cereb Cortex. 2014;24:2210–8. doi:10.1093/cercor/bht076.
39. Camus V, Payoux P, Barre L, Desgranges B, Voisin T, Tauber C, et al. Using PET with 18F-AV-45 (florbetapir) to quantify brain amyloid load in a clinical environment. Eur J Nucl Med Mol Imaging. 2012;39:621–31. doi:10.1007/s00259-011-2021-8.
40. Poisnel G, Herard AS, El Tannir El Tayara N, Bourrin E, Volk A, Kober F, et al. Increased regional cerebral glucose uptake in an APP/PS1 model of Alzheimer's disease. Neurobiol Aging. 2012;33:1995–2005. doi:10.1016/j.neurobiolaging.2011.09.026.
41. Puzzo D, Privitera L, Leznik E, Fa M, Staniszewski A, Palmeri A, et al. Picomolar amyloid-beta positively modulates synaptic plasticity and memory in hippocampus. J Neurosci. 2008;28:14537–45. doi:10.1523/JNEUROSCI.2692-08.2008.
42. Magistretti PJ, Pellerin L. Cellular mechanisms of brain energy metabolism and their relevance to functional brain imaging. Philos Trans R Soc Lond B Biol Sci. 1999;354:1155–63.
43. Shankar GM, Bloodgood BL, Townsend M, Walsh DM, Selkoe DJ, Sabatini BL. Natural oligomers of the Alzheimer amyloid-beta protein induce reversible synapse loss by modulating an NMDA-type glutamate receptor-dependent signaling pathway. J Neurosci. 2007;27:2866–75. doi:10.1523/JNEUROSCI.4970-06.2007.

44. Cirrito JR, Kang JE, Lee J, Stewart FR, Verges DK, Silverio LM, et al. Endocytosis is required for synaptic activity-dependent release of amyloid-beta in vivo. Neuron. 2008;58:42–51. doi:10.1016/j.neuron.2008.02.003.
45. Buckner RL, Sepulcre J, Talukdar T, Krienen FM, Liu H, Hedden T, et al. Cortical hubs revealed by intrinsic functional connectivity: mapping, assessment of stability, and relation to Alzheimer's disease. J Neurosci. 2009;29:1860–73. doi:10.1523/JNEUROSCI.5062-08.2009.
46. Choi SR, Schneider JA, Bennett DA, Beach TG, Bedell BJ, Zehntner SP, et al. Correlation of amyloid PET ligand florbetapir F 18 binding with Abeta aggregation and neuritic plaque deposition in postmortem brain tissue. Alzheimer Dis Assoc Disord. 2012;26:8–16. doi:10.1097/WAD.0b013e31821300bc.
47. Deshpande A, Kawai H, Metherate R, Glabe CG, Busciglio J. A role for synaptic zinc in activity-dependent Abeta oligomer formation and accumulation at excitatory synapses. J Neurosci. 2009;29:4004–15. doi:10.1523/JNEUROSCI.5980-08.2009.
48. Besson FL, La Joie R, Doeuvre L, Gaubert M, Mezenge F, Egret S, et al. Cognitive and brain profiles associated with current neuroimaging biomarkers of preclinical Alzheimer's disease. J Neurosci. 2015;35:10402–11. doi:10.1523/JNEUROSCI.0150-15.2015.
49. Ossenkoppele R, Tolboom N, Foster-Dingley JC, Adriaanse SF, Boellaard R, Yaqub M, et al. Longitudinal imaging of Alzheimer pathology using [11C]PIB, [18F]FDDNP and [18F]FDG PET. Eur J Nucl Med Mol Imaging. 2012;39:990–1000. doi:10.1007/s00259-012-2102-3.
50. Morbelli S, Garibotto V, Van De Giessen E, Arbizu J, Chetelat G, Drezgza A, et al. A Cochrane review on brain [18F]FDG PET in dementia: limitations and future perspectives. Eur J Nucl Med Mol Imaging. 2015;42:1487–91. doi:10.1007/s00259-015-3098-2.
51. Thomas BA, Erlandsson K, Modat M, Thurfjell L, Vandenberghe R, Ourselin S, et al. The importance of appropriate partial volume correction for PET quantification in Alzheimer's disease. Eur J Nucl Med Mol Imaging. 2011;38:1104–19. doi:10.1007/s00259-011-1745-9.
52. Erlandsson K, Buvat I, Pretorius PH, Thomas BA, Hutton BF. A review of partial volume correction techniques for emission tomography and their applications in neurology, cardiology and oncology. Phys Med Biol. 2012;57:R119–59. doi:10.1088/0031-9155/57/21/R119.
53. Quarantelli M, Berkouk K, Prinster A, Landeau B, Svarer C, Balkay L, et al. Integrated software for the analysis of brain PET/SPECT studies with partial-volume-effect correction. J Nucl Med. 2004;45:192–201.
54. Labbe C, Froment JC, Kennedy A, Ashburner J, Cinotti L. Positron emission tomography metabolic data corrected for cortical atrophy using magnetic resonance imaging. Alzheimer Dis Assoc Disord. 1996;10:141–70.
55. Samuraki M, Matsunari I, Chen WP, Yajima K, Yanase D, Fujikawa A, et al. Partial volume effect-corrected FDG PET and grey matter volume loss in patients with mild Alzheimer's disease. Eur J Nucl Med Mol Imaging. 2007;34:1658–69. doi:10.1007/s00259-007-0454-x.
56. Su Y, Blazey TM, Snyder AZ, Raichle ME, Marcus DS, Ances BM, et al. Partial volume correction in quantitative amyloid imaging. Neuroimage. 2015;107:55–64. doi:10.1016/j.neuroimage.2014.11.058.
57. Brendel M, Hogenauer M, Delker A, Sauerbeck J, Bartenstein P, Seibyl J, et al. Improved longitudinal [(18)F]-AV45 amyloid PET by white matter reference and VOI-based partial volume effect correction. Neuroimage. 2015;108:450–9. doi:10.1016/j.neuroimage.2014.11.055.